# Waterborne Hyperbranched Polyurethane/Nickel Ferrite Decorated Reduced Graphene Oxide Nanocomposite

## *Highlight*

This chapter demonstrates *in situ* fabrication of tannic acid based waterborne hyperbranched polyurethane nanocomposite using nickel ferrite decorated reduced graphene oxide nanohybrid. Nickel ferrite decorated reduced graphene oxide was prepared through a hydrothermal method. The prepared nanohybrid and nanocomposite were characterized by using different spectroscopic and analytical techniques such as FTIR, XRD, Raman and TEM analyses. Various properties of the nanocomposite were also evaluated. The nanocomposite exhibited excellent thermal stability (initial degradation temperature up to 355 °C) and good mechanical properties (tensile strength 24.2 MPa, elongation at break 280% and toughness 33.05 MJ $m^{-3}$). The nanocomposite also exhibited outstanding multi-stimuli responsive shape memory behavior under thermal, sunlight and microwave (300 W) irradiation. The performance of the nanocomposite was found to be dependent on the nanomaterial loading. Thus, the study showed that developed nanocomposite can be used as a high performance, non-contact triggered smart material for advanced shape memory application.

---

Parts of this chapter are published in

**Gogoi, S.**, & Karak, N. Biobased waterborne hyperbranched polyurethane/$NiFe_2O_4$@rGO nanocomposite with multi-stimuli responsive shape memory attributes, *RSC Adv.* **6**, 94815--94825, 2016.

## 7.1. Introduction

Among various carbonaceous nanostructures, graphene based materials have received substantial attention in the domain of material research. Graphene nano-sheets (GNs) are composed of extremely thin, 2-D honeycomb lattices of carbon atoms. They possess unique properties like high Young's modulus (~1 TPa), large theoretical specific surface area (2630 $m^2$ $g^{-1}$), excellent thermal conductivity (3000–5000 W $mK^{-1}$), high carrier mobility (~10,000 $cm^2$ $Vs^{-1}$) and good optical transmittance (~97.7%).[1-4] Hence, graphene has been used as nanomaterial for different polymeric materials. In this context, present chapter made an effort to utilize reduced graphene oxide (rGO) based nanohybrid system to develop nanocomposite of tannic acid based hyperbranched waterborne polyurethane (WHPU) with shape memory attribute.

Shape memory polymers belong to "smart" class of materials which are attracting copious interest for many advanced applications, such as functional textiles, smart customer products, active aircraft equipment, adaptive biomedical devices, interactive electronic apparatuses etc.[5-9] This type of material possesses the ability to switch in to a fixed temporary deformed state, which can be switched off to the original shape by using certain stimuli.[10] Among various polymeric materials, polyurethane (PU) has been considered as one of the most promising candidates for shape memory application due to its high recoverable strain, wide range of transition temperature for shape recovery and high control of retraction and softening temperature.[11-13] PU consists of soft and hard domains, in which the former and later constitute the reversible and frozen phase, respectively. The reversible phase is responsible for holding the temporary deformation, while the frozen phase containing physical or chemical cross-linked points is responsible for memorizing the permanent shape. In real practice, there exists a transition temperature ($T_{trans}$) with respect to which shape fixation and recovery can be achieved.

In conventional SMP, shape recovery is achieved by direct heating the polymer above $T_{trans}$. However, in recent time, stress has been given on the use of indirect heating devices by applying non-contact and remote triggers for shape recovery. In this perspective, PU nanocomposites have been studied extensively.[14-18] Nanomaterials which respond specifically against certain

stimulus can be used to develop such PU nanocomposites. Nanomaterials like carbon nanotube, carbon fiber, graphene, iron oxide, silicon carbide etc. have been reportedly utilized in stimuli responsive shape memory polymer by using triggers of electrical field, magnetic field, microwave, UV light etc.[19-27] In the present study we choose to use nickel ferrite ($NiFe_2O_4$) decorated rGO ($NiFe_2O_4$@rGO) nanohybrid for the fabrication of WHPU. Such a nanohybrid system contains both electrically and magnetically active components. Therefore, it is expected that it will sufficiently interact with different regions of electromagnetic radiation including microwave and visible light. Graphene being a conductor of heat can allocate absorbed energy within the matrix uniformly, which may result effective remote heating of the polymer matrix and bring about efficient shape recovery.

Therefore, present study reports hydrothermal preparation of $NiFe_2O_4$@rGO nanohybrid. Different weight percentages of this nanohybrid were used to fabricate nanocomposites of WHPU (WHPU/$NiFe_2O_4$@rGO) by following an *in situ* polymerization technique. Both the nanohybrid and nanocomposite were characterized by using different spectroscopic and analytical techniques. Different properties such as thermal, mechanical etc. were also evaluated. The developed system was tested as a shape memory material by using different external stimuli like thermal energy, microwave and sunlight.

## 7.2. Experimental

### 7.2.1. Materials

IPDI, PEG 600 and BD of similar grade and specifications were used as described in Sub-Chapter 2A (Section 2A.2.1.). Likewise, other chemicals including BMPA, TA, TEA and THF were used in the fabrication of WHPU/$NiFe_2O_4$@rGO nanocomposite with similar grade and specifications as described in Sub-Chapter 2B (Section 2B.2.1.). Same HE and PAA as mentioned in Chapter 3 (Section 3.2.1.) were used in the modification of the nanocomposite films.

On the other hand, graphitic powder of synthetic grade having particle size <20 μm was procured from Sigma-Aldrich, Germany. It possesses m.w. of

12 g $mol^{-1}$ and m.p. of 3652-3697 °C. Iron(III) chloride hexahydrate ($FeCl_3.6H_2O$) with 97% assay was purchased from Sigma-Aldrich, Germany. It has m.w. of 270.3 g $mol^{-1}$, m.p. of 37 °C and b.p. of 285 °C. Nickel(II) chloride hexahydrate ($NiCl_2.6H_2O$) with 98% assay was obtained from Sigma-Aldrich, Germany. It has m.w. of 237.69 g $mol^{-1}$ and m.p. of 1001 °C. Tri-sodium acetate ($Na_3C_6H_5O_7$) with m.w. of 294.10 g $mol^{-1}$, m.p. of 150 °C and s.g. of 1.76 (at 20 °C) was purchased from Merck, India. Potassium permanganate ($KMnO_4$) with m.w. of 158.03 g $mol^{-1}$ and m.p. of 240 °C was procured from Merck, India. 30% Hydrogen peroxide ($H_2O_2$) was procured from, Merck, India which has m.w. of 34.01 g $mol^{-1}$, b.p. of 107 °C, m.p. of -26 °C and s.g. of 1.11 (at 20 °C). 98% Sulphuric acid (~18.4 M) was obtained from Merck, India. It has m.w. of 98.08 g $mol^{-1}$, b.p. of 335 °C, m.p. of -20 °C and s.g. of 1.84 (at 20 °C).

### 7.2.2. Characterization

FTIR spectra of the nanohybrid and nanocomposite were recorded under same condition using the same spectrometer as stated in Sub-Chapter 2A (Section 2A.2.2.). The shape, size and decoration of $NiFe_2O_4$@rGO, as well as its distribution over the polymer matrix were visually studied by TEM analysis using the same instrument and grid as mentioned in Chapter 4 (Section 4.2.2.). The microscopic data were analyzed for FFT and IFFT images by using Gatan Microscopy Suite Software as mentioned in the same chapter. Same instruments and experimental conditions were deployed for other characterizations of the nanohybrid and polymeric nanocomposite, which include EDX for elemental analysis, XRD for diffraction patterns and Raman spectroscopy for study of graphitic structure as described in Chapter 4 (Section 4.2.2.). Likewise, for the evaluation of thermal and mechanical properties, same instruments and instrumentation techniques such TGA, DSC, UTM, scratch hardness tester, impact tester, gloss meter etc. were used as described in Sub-Chapter 2A (Section 2A.2.2.). A domestic microwave oven LG, India was used in the study of shape memory behavior of the nanocomposite at a power of 300 W.

### 7.2.3. Methods

#### *7.2.3.1. Preparation of $NiFe_2O_4$@rGO*

Graphene oxide (GO) was prepared by the oxidation of graphitic powder according to modified Hummers' method.[27] Accordingly, 2 g of graphitic powder was subjected to acid treatment with 35 mL of 98% $H_2SO_4$ under constant stirring for 1 h. It was followed by addition of 6 g of $KMnO_4$ to this mixture very slowly and cautiously at temperature below 20 °C. When evolved heat subsides, the mixture was vigorously stirred at 35 °C for 4 h. Then it was diluted with 90 mL of water under cool and stirring condition. After 1 h, a dark brown colored solution was observed. To this solution 30% $H_2O_2$ was added dropwise until the color turned into bright yellow. From this solution, GO was separated out by centrifuge technique, which was purified by subsequent washing with 5% HCl solution and water for several cycles. This GO was dried inside an oven at 50 °C for 3 h. In order to prepare $NiFe_2O_4$@rGO nanohybrid, an aqueous dispersion of GO (1.0 g) was prepared by using ultra-sonication to which 1.04 g of $FeCl_3.6H_2O$ and 2.31 g of $NiCl_2.6H_2O$ were added. 100 mg of tri-sodium acetate was also added as chelating agent. This mixture was stirred for 1 h and then poured into a Teflon lined hydrothermal reactor. It was subjected to a temperature of 180 °C for 10 h.[28] After the completion of the process, $NiFe_2O_4$@rGO nanohybrid was separated by centrifugation and washed with ethanol (to remove tri-sodium acetate) and water several times. Then it was dried inside an oven at 50 °C for 5 h.

#### *7.2.3.2. Fabrication of WHPU/$NiFe_2O_4$@rGO nanocomposite*

WHPU/$NiFe_2O_4$@rGO nanocomposite was prepared by following an *in situ* technique. Briefly, IPDI, PEG 600 and BMPA were allowed to react under nitrogen flow at 80±2 °C for 1.5 h inside a four neck glass reactor equipped with a mechanical stirrer, a nitrogen gas inlet and a condenser. Functional ratio of -NCO/-OH was maintained at 1.5. In the next step, BD and TA were added to the reaction mixture at room temperature using THF as the solvent (maintaining -NCO/-OH=1.1). Then the reaction was continued at 70±2 °C for 3.5 h. After completion of this step, BD and $NiFe_2O_4$@rGO were introduced into the reaction by maintaining -NCO/-OH ratio one. Further reaction was carried

out for another 1.5 h at 70±2 °C. Then, the polymeric solution was allowed to cool. When temperature felt below 25 °C, TEA was introduced very slowly with constant mechanical stirring for 30 min. Consequently, water was added at a very slow rate maintaining strong mechanical agitation. Then THF was removed under reduced pressure. Different weight percentages of $NiFe_2O_4$@rGO, *viz.* 0.5, 1.0, 1.5 and 2.0 wt% were used to prepare different compositions of the nanocomposite, which were coded as PNC0.5, PNC1.0, PNC1.5 and PNC2.0, respectively. To prepare the films, these compositions were mixed with 10 wt% of HE and 5 wt% of PAA by ultra-sonication, which were then cast on glass plates, dried under atmospheric condition and heated at 100 °C for 45 min. Films were finally peeled off and used for various testing. Different properties of the nanocomposites were compared with a pristine system, which is equivalent to MWPU10 as described in Chapter 3. However, a general coding, i.e. MWPU has been adopted for MWPU10 in this chapter.

#### *7.2.3.3. Shape memory behavior*

The study of shape memory effect of polymeric nanocomposite consists of two processes, *viz.* shape fixation and shape recovery.[28] The shape fixation of the tested films was carried out through a series of thermal cyclic experiments. Briefly, the films were given a spiral shape by folding them at temperature $T_m$+20 °C (~60 °C). This deformed state was fixed by subjecting the spiral shaped films instantaneously into an ice cool bath (temperature 5±1 °C) for 15 min. Then, the temporarily fixed samples were dried inside a vacuum oven at room temperature (25 °C) and kept for 30 min. Thereafter, shape recovery of the temporarily folded nanocomposite films was carried out by using different stimuli, *viz.* thermal energy, microwave and sunlight. For, thermally induced shape recovery, the samples were directly heated in a water bath at 40 °C temperature and time required to retain the original shape was recorded. Similarly, microwave triggered shape recovery effect was studied by putting the samples inside a domestic microwave at a power of 300 W. For sunlight induced shape recovery, samples were irradiated directly under sunlight in a thermostat maintaining a constant temperature of 25 °C. The light intensity was measured as ~80,000-90,000 lux. In all the experiments, time of shape recovery was recorded. Also, in order to express effectiveness of these

polymeric nanocomposites as shape memory material, quantitative evaluation was made in terms of percentage shape fixity and recovery by using the following equations:[28]

$$\text{Shape recovery (\%)} = \frac{90 - \theta}{90} \times 100 \ldots\ldots\ldots\ldots\ldots\ldots\ldots\ldots (\mathbf{Eq.\ 7.1})$$

$$\text{Fixity (\%)} = \frac{\theta}{90} \times 100 \ldots\ldots\ldots\ldots\ldots\ldots\ldots\ldots\ldots\ldots\ldots (\mathbf{Eq.\ 7.2})$$

where, θ in degrees denotes the angle between the tangential line at the midpoint of the sample and the line connecting the midpoint and the end of the curved sample. Shape memory test was performed in triplicate for all the compositions.

## 7.3. Results and discussion

### 7.3.1. Preparation of $NiFe_2O_4$@rGO

Hydrothermal method was found fruitful to prepare $NiFe_2O_4$@rGO nanohybrid system. Initial ultra-sonication of GO solution resulted exfoliation of the stacked structure. This helped to bring a proper interaction between GO, $NiFe_2O_4$ precursors and chelating agent during the mixing process. Generally, the basal plane of GO contains hydroxyl and epoxy groups, whereas the carboxylic groups are present on the edges. The oxygen functional groups of GO played the anchoring role in the formation of $NiFe_2O_4$@rGO nano-sheets. In a plausible mechanistic route as depicted in **Scheme 7.1**, it is considered that GO undergoes an interaction with the metallic precursors of $NiFe_2O_4$ through these oxygen functional groups. This happened through either dative bonding or ionic interactions. These absorbed Fe and Ni ions on GO sheets acted as the sites for nucleation. On the other hand, tri-sodium citrate which was used as the chelating agent, bound rest of the Fe(III) and Ni(II) present in the system forming citrate complexes. Upon subjecting into a hydrothermal condition, [Fe(citrate)] and $[Ni(citrate)]^-$ complexes got weaken and gradually released Fe(III)/Ni(II) to the nucleation site. This helped to achieve a controlled nucleation and crystal growth process over the GO sheets. In the final stage of the hydrothermal process, Ni(II) and Fe(III) integrated at the nucleation sites to form $NiFe_2O_4$ phase. In addition to act as binder, tri-sodium acetate also

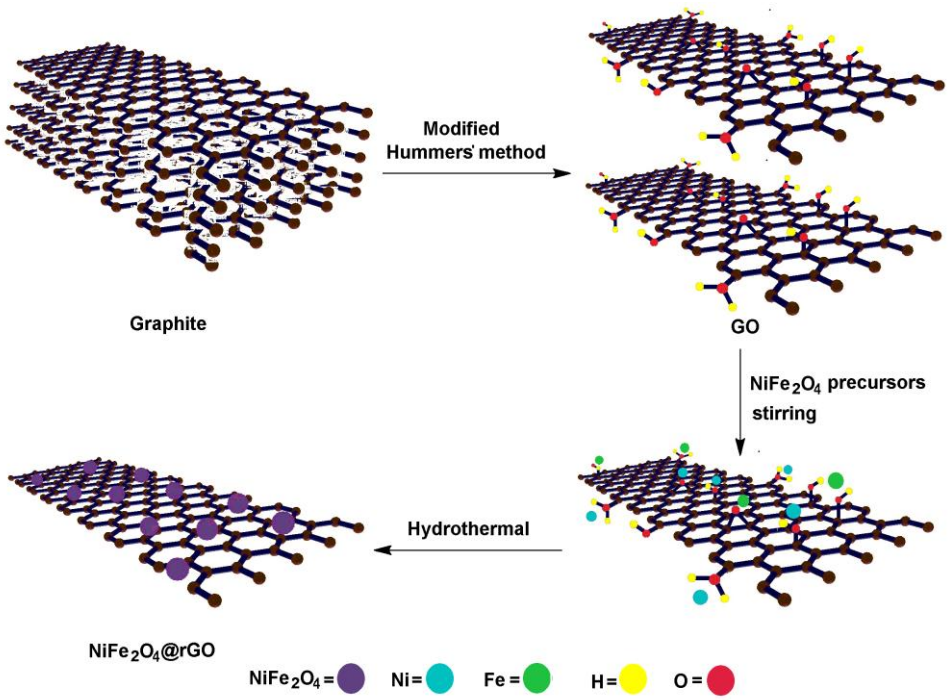


**Scheme 7.1.** Plausible mechanism for the formation of NiFe$_2$O$_4$@rGO nanohybrid.

served as the reducing agent for GO. Literature showed that under hydrothermal condition tri-sodium acetate oxidized into dicarboxy acetone.[29] Electrons released in this process were accepted by GO and utilized in the reduction of various functional groups. Moreover, hydrothermal method causes thermal reduction of GO as well. Under hydrothermal condition extensive decarboxylation and dehydration take place at the defect sites.[30] This caused aromatization and thus helped in the formation of a nearly perfect graphitic structure in the form of rGO. Thus, the overall process was found effective to obtain NiFe$_2$O$_4$@rGO nanohybrid.

### 7.3.2. Characterization of NiFe$_2$O$_4$@rGO

The prepared NiFe$_2$O$_4$@rGO nanohybrid was characterized for structural confirmation. FTIR study revealed the presence of different functionalities in the nanohybrid system (**Figure 7.1a**). The band near 3400 cm$^{-1}$ is assigned to the -O-H stretching vibration of absorbed moisture entrapped within NiFe$_2$O$_4$ crystal structure. On the other hand, peaks appeared at frequencies 488 and 670 cm$^{-1}$ are attributed to Fe-O deformation vibrations. Appearance of these two peaks is significant. They are considered as the major metal-oxygen

vibrations that occurred in $NiFe_2O_4$ crystal.[31,32] On the other hand, peak at 1604 $cm^{-1}$ is assigned for -C=C- stretching of rGO structure. Likewise, very weakly intense peaks near 2900 $cm^{-1}$ and 1720 $cm^{-1}$ region can be attributed to -C-H and -C=O stretching frequencies, respectively. These were originated from the defect sites that exist within the graphitic structure of rGO. Weak peak intensities of these peaks confirmed the presence of graphene in the reduced form. Thus, FTIR spectral data furnished preliminary idea about the formation of $NiFe_2O_4$@rGO nanohybrid system. XRD study was also carried out to confirm the formation of $NiFe_2O_4$ phase in the nanohybrid system (**Figure 7.1b**). XRD technique is useful for the investigation of phase purity of a system. The XRD pattern as shown in **Figure 7.1b** confirmed $NiFe_2O_4$ present in the nanohybrid. XRD peaks at 2θ values of 18.4°, 30.3°, 35.7°, 43.4°, 53.5°, 57.4° and 63.1° are indexed as (111), (220), (311), (400), (422), (511) and (440) crystal planes of $NiFe_2O_4$, respectively. The crystallographic data are confirmed by comparing with the data obtained from ICDD-PDF-2 (data card number 86-2267). On the other hand, (011) and (022) peaks of rGO almost disappeared in the XRD diffractogram. This may happen due to the intercalation of $NiFe_2O_4$ within the graphic layers during crystal growth process, which results rupturing of regular graphitic stacking. Further, high intensity of $NiFe_2O_4$ crystal diffraction may also results diminishing of rGO diffraction intensity. Raman analysis was performed in order to detect the presence of rGO phase in the nanohybrid system. Raman is quite helpful for detection of disorder present in the graphitic structure. From the Raman spectrum of $NiFe_2O_4$@rGO nanohybrid two distinct bands, *viz.* D and G were identified. The D band at 1342 $cm^{-1}$ corresponds to the defects present in the graphitic structure, while G band at 1592 $cm^{-1}$ represents graphitic $sp^2$ symmetric carbon stretching (**Figure 7.1c**). Moreover, compared to the band positions of GO, D and G band in rGO suffered a blue-shift. This is an indicative of reduction of GO into rGO.[33] The relative intensity ratio of D and G band supports the fact. $I_D/I_G$ ratio was found to be decreased in the nanohybrid system compared to GO. Hence, it confirmed an effective reduction of GO during the hydrothermal process as described in the earlier section. Further, a 2D band at 2870 $cm^{-1}$ was observed in the Raman spectrum of $NiFe_2O_4$@rGO, which was not present in GO. This has raised due

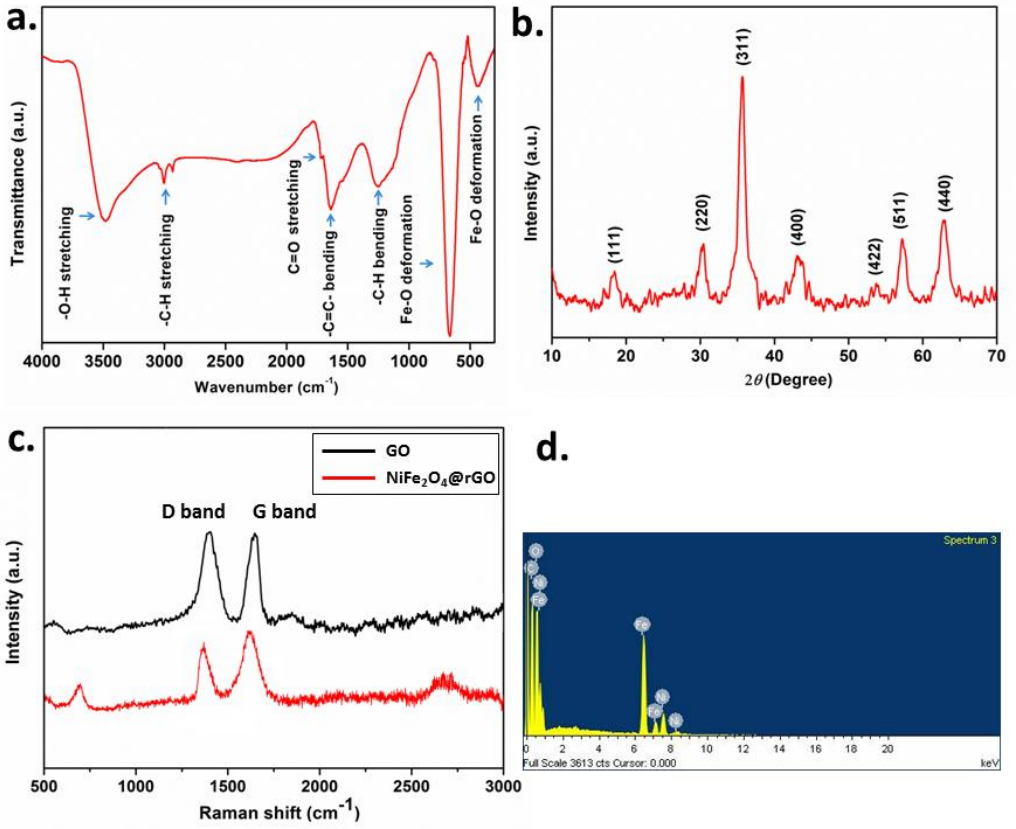


**Figure 7.1. (a)** FTIR spectrum of $NiFe_2O_4$@rGO, **(b)** XRD pattern of $NiFe_2O_4$@rGO, **(c)** Raman spectra of GO and $NiFe_2O_4$@rGO and **(d)** EDX spectrum of $NiFe_2O_4$@rGO.

to the formation of graphene structures. Besides, confirming the presence of rGO phase in the nanohybrid, Raman analysis also reveals the formation of $NiFe_2O_4$ phase. The multiple peaks appeared in 500-800 $cm^{-1}$ region can be assigned for metal vibration of $NiFe_2O_4$ phase.[34] Thus, Raman spectrum of $NiFe_2O_4$@rGO confirmed the formation of both the inorganic and carbon based phase during the hydrothermal preparation. SEM/EDX study confirmed the presence of Ni, Fe, O and C in the nanohybrid system (**Figure 7.1d**). Morphological study of the nanohybrid including shape, size and distribution was carried out through visual analysis using TEM as the tool. TEM images depicted in **Figure 7.2a** and **b** confirmed decoration of $NiFe_2O_4$ over rGO sheets. However, small agglomeration of $NiFe_2O_4$ can be observed due to its paramagnetic behavior. Nevertheless, a stable and controlled decoration was perceived through the hydrothermal preparation as evidenced by TEM pictures. Statistical analysis reveals that the size distribution lies in between 5-13 nm (**Figure 7.2c**). The largest fraction of $NiFe_2O_4$ particles possessed size in

the range of 7-10 nm. TEM image also shows edge of rGO sheets (**Figure 7.2d**). HRTEM image shows that the magnetic nanoparticles possess near hexagonal shape (**Figure 7.2e** and **f**). HRTEM image of $NiFe_2O_4$ further shows the presence of lattice fringes. Conversion of selected area of **Figure 7.2f** into corresponding IFFT image reveals two different inter-planar distances (**Figure 7.2h**). Here, *d* value of 0.291 nm can be ascribed for (220) lattice plane, while that of 0.249 nm is assigned for (311) crystallographic plane of $NiFe_2O_4$. SAED pattern of the nanohybrid shows concentric circles with bright spots indicating the presence of crystalline structure (**Figure 7.2g**). FFT image also provides valuable information about the crystal phase of the nanohybrid system (**Figure 7.2i**). From the FFT image (220), (400) and (440) planes of $NiFe_2O_4$ are identified. On the other hand, **Figure 7.3** shows the magnetic behavior of the nanohybrid under the influence of an ordinary magnet.

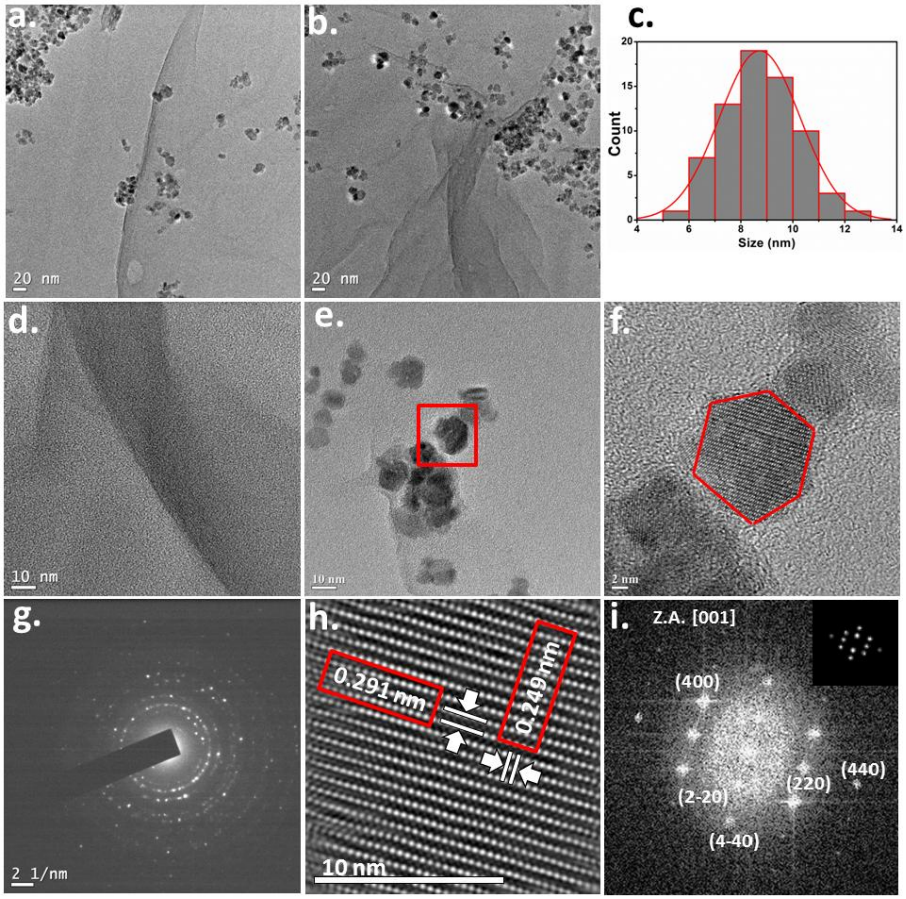


**Figure 7.2. (a)** and **(b)** TEM images of $NiFe_2O_4$@rGO; **(c)** Size distribution of $NiFe_2O_4$; **(d)** Edge of rGO sheets; **(e)** and **(f)** HRTEM of $NiFe_2O_4$ phase; **(g)** SAED pattern of $NiFe_2O_4$@rGO; **(h)** IFFT image of $NiFe_2O_4$ phase; **(i)** FFT image of $NiFe_2O_4$ phase (inset FFT after masking).

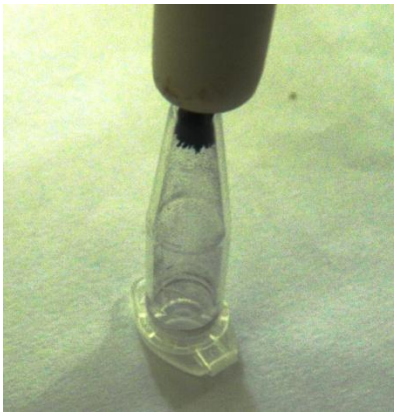

**Figure 7.3.** Magnetic behavior of $NiFe_2O_4$@rGO under the magnetic field of an ordinary magnet.

### 7.3.3. Fabrication of WHPU/$NiFe_2O_4$@rGO nanocomposite

WHPU was fabricated with the prepared nanohybrid by following an *in situ* polymerization technique. Generally, compatibility and state of dispersibility of nanomaterial greatly influence various properties of polymeric nanocomposite.[35] Hence, in the fabrication process maximum care was taken to ensure formation of a homogenously distributed WHPU/$NiFe_2O_4$@rGO nanocomposite. In the present study, we found both the nanomaterial and polymer matrix complementing each other to achieve such a highly compatible and uniformly distributed system. The common problem associated with the fabrication of conventional PU/graphene system is poor compatibility between both.[36] However, we found WHPU matrix suitable for this purpose. WHPU contains a large number of -COOH groups along the polymeric chains. These were incorporated as ionic centers along with the internal emulsifier BMPA. In the neutralization step (as mentioned in the preparative method) by adding TEA, these groups were converted into carboxylate ions. These ionic centers played a key role to bring a homogeneous dispersion of $NiFe_2O_4$@rGO over the polymer matrix. It is proposed that metallic part of $NiFe_2O_4$ went into a strong interaction with the negatively charged carboxylate groups of the polymer chains as shown in **Scheme 7.2**. At this juncture, it is pertinent to mention that BMPA was reacted in the very first step, which ensures a uniform distribution of -COOH groups along the polymeric arms. Similarly, $NiFe_2O_4$ were found decorated uniformly over rGO sheets. Thus, absorption of $NiFe_2O_4$@rGO over

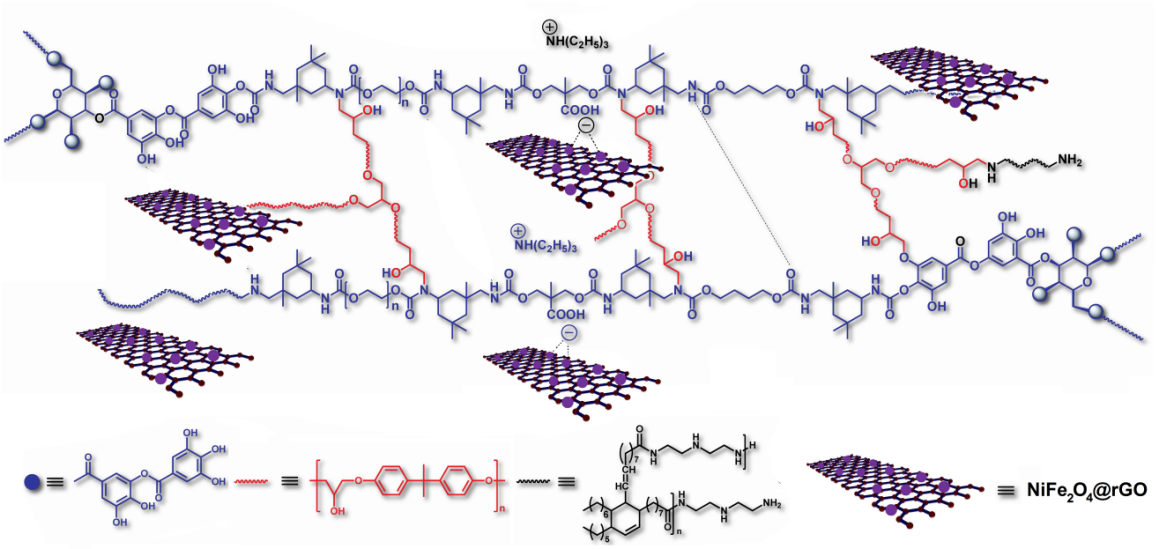


**Scheme 7.2.** Schematic presentation of *in situ* fabricated WHPU/NiFe$_2$O$_4$@rGO nanocomposite.

the polymer matrix through metal/COO$^-$ interaction leads to a uniformly distributed and highly compatible polymeric nanocomposite system. Further, NiFe$_2$O$_4$@rGO was incorporated during the chain extension process. Such tactic seemed to be effective as nanomaterial can rather easily penetrate low viscus growing polymeric chains under the reaction condition. Moreover, incorporation of the nanohybrid during polymerization reaction helped to achieve a strong interaction during the neutralization step through an *in situ* mechanism. TEM image of PNC2.0 confirmed a uniform distribution of NiFe$_2$O$_4$@rGO even at a high loading (**Figure 7.4a** and **b**). FTIR spectra as shown in **Figure 7.5** confirmed various functional groups present in the nanocomposite system, which include 3400 cm$^{-1}$ for -O-H stretching, 2900-3000 cm$^{-1}$ for -C-H stretching, 1710-1740 cm$^{-1}$ for -C=O stretching, 1615 cm$^{-1}$ for -C=C- stretching, 1470 cm$^{-1}$ for -C-H bending, 1120 cm$^{-1}$ for -C-O stretching and 488 cm$^{-1}$ for Fe-O deformed vibration. On the other hand, modification of these nanocomposites with HE and PAA helped to create additional cross-linking points within the system, which contributed significantly to form a dimensionally stable structure. In context of shape memory application, such system may prove worthy to memorize the permanent shape of the material.

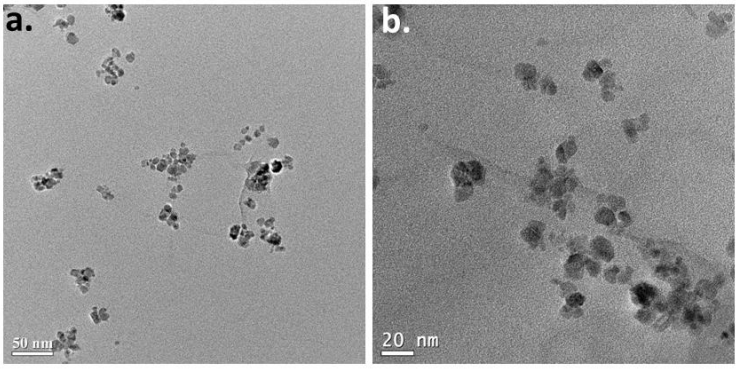


**Figure 7.4. (a)** and **(b)** TEM images of PNC2.0.

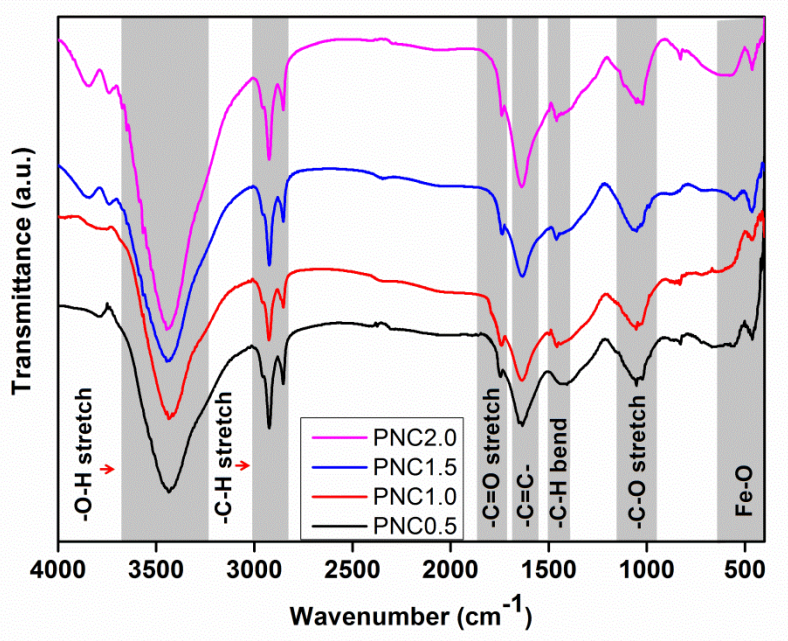


**Figure 7.5.** FTIR spectra of PNCs.

### 7.3.4. Mechanical properties

Mechanical properties of the polymeric nanocomposite were evaluated and results are given in **Table 7.1**. It has been found that incorporation of NiFe$_2$O$_4$@rGO to WHPU reinforced most of the mechanical properties such as tensile strength, toughness, impact resistance, scratch hardness etc. Further, such improvement was found to be dependent on nanomaterial loading. As a nanomaterial, rGO possesses several favorable attributes like high mechanical strength (tensile strength 125 MPa and tensile modulus 1100 GPa), high aspect ratio, two dimensional geometry etc.[1,31] These factors contributed significantly towards improved performance of WHPU/NiFe$_2$O$_4$@rGO nanocomposite.

**Table 7.1.** Mechanical properties of WHPU/$NiFe_2O_4$@rGO nanocomposite

| Property* | Composition | | | | |
|---|---|---|---|---|---|
| | MWPU# | PNC0.5 | PNC1.0 | PNC1.5 | PNC2.0 |
| TS (MPa) | 11.8±0.6 | 14.7±0.7 | 16.9±08 | 19.0±0.4 | 24.2±0.5 |
| E@B (%) | 292±1 | 289±2 | 291±4 | 294±2 | 280±3 |
| Toughness§ (MPa) | 25.2 | 27.92 | 30.74 | 33.42 | 33.05 |
| SH† (kg) | 7.5±0.2 | 8.5±0.3 | 9.0±0.2 | 9.8±0.1 | >10 |
| IR‡ (kJ $m^{-1}$) | 7.47±0.15 | 7.90±0.2 | 8.11±0.15 | >8.30 | >8.30 |
| Bending¶ (m) | 0.002 | 0.002 | 0.002 | 0.002 | 0.003 |
| Gloss (60°) | 95.5±0.5 | 88.7±0.8 | 87.4±0.8 | 87.7±0.5 | 86.3±0.2 |

**Mechanical properties: TS=Tensile strength, E@B=Elongation at break, SH=Scratch hardness, IR=Impact resistance; §Obtained by calculating area under stress-strain curve; †Limit of scratch hardness tester was 10 kg (maximum); ‡Limit of impact tester is 8.30 kJ $m^{-1}$ for film of thickness 1mm (maximum); ¶Limit of the mandrel diameter was 1 mm (minimum). #Data presented from Chapter 3 for comparison.*

$NiFe_2O_4$ decorated rGO sheets provided a better adhesion of two dimensional graphene sheets into the WHPU matrix as described in the section 7.3.3. This facilitates efficient load transfer between rGO nano-sheets and the WHPU matrix. Further, very strong secondary interactions exists within the polymeric structure in the form of H-bonding, π-π stacking, van-der-Waals' interaction etc. These forces also played an important role towards improved mechanical properties by providing structural stiffness. Thus, as a consequence of all these factors, very good mechanical performance of WHPU/$NiFe_2O_4$@rGO nanocomposite was perceived. However, elongation at break values were found to follow an irregular trend. Up to 1.5 wt% of the nanomaterial loading, elongation at break values were increased, though increment was not very substantial. At 2.0 wt% of $NiFe_2O_4$@rGO, elongation at break value was found decreasing. From such observations, it can be concluded that at low loading of nanomaterial (<1.5 wt%), the nanohybrid acted favorably enhancing both tensile strength and elongation at break values. This can be attributed to the layered structure of rGO, which slipped under applied stress.[11] But, at high loading (>1.5 wt%) such effect has only nominal contribution, as the crowded

nanomaterial imparts very high structural rigidity to the polymer matrix. Under such circumstances, slipping of graphene layers no longer overcome the stiffness of the system. As a result, elongation at break value decreased. However, all the compositions of WHPU/$NiFe_2O_4$@rGO nanocomposite possessed very good flexibility as reflected by the bending values. Similarly, gloss values were found good for all the compositions.

### 7.3.5. Thermal properties

Various thermal properties of WHPU/$NiFe_2O_4$@rGO have been evaluated. TG study showed improvement of thermal stability of the pristine system by the formation of nanocomposite. TG thermograms undergo a shift towards higher temperature with increase in $NiFe_2O_4$@rGO content in the polymer matrix (**Figure 7.6a**). Such improvement can be attributed to the presence of metal decorated rGO sheets in the nanocomposite system. The nanomaterial in the polymer occupied the free space and made the system more rigid. This delayed the molecular thermal chain motion leading to enhance thermal stability. Further, metallic $NiFe_2O_4$ possesses very high thermal stability. They acted as a thermal barrier against the volatile decomposed products escaping from the polymer system and thereby delaying the degradation process. Likewise, char produced as a result of thermal decomposition of rGO served as thermal insulator, which tends to protect the non-degraded polymer from further thermal degradation. Besides the role of nanomaterial, the secondary interactions like H-bonding, π-π interaction, van der waals' attraction etc. also played crucial role towards improved thermal stability of WHPU/$NiFe_2O_4$@rGO nanocomposite as described in the earlier chapters. On the other hand, $T_g$ of the nanocomposite was found to follow an increasing trend with increase amount of nanomaterial content (**Figure 7.6b**). This confirms the stiffness imparted by $NiFe_2O_4$@rGO to the polymer structure. Further, melting point ($T_m$) was also found increasing by the incorporation of $NiFe_2O_4$@rGO (**Figure 7.6c**). Thus, a positive improvement of thermal properties was perceived. All such results agreed the previous observations made by Thakur and Karak while studying PU nanocomposites with graphene based nanomaterials.[11,27]

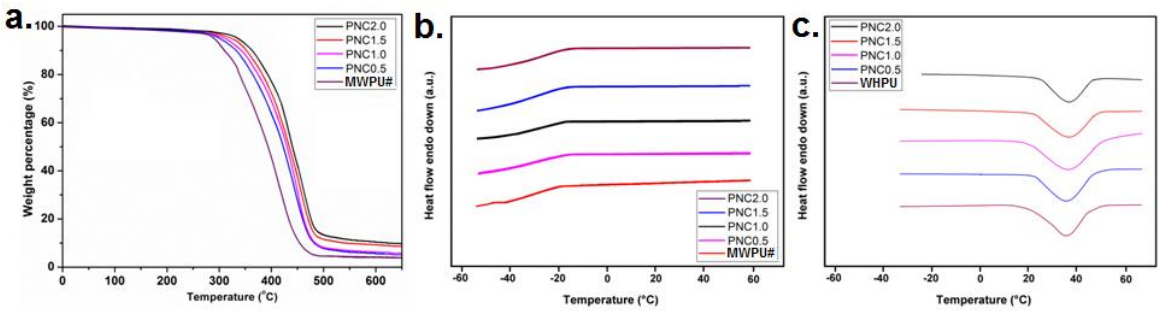


**Figure 7.6. (a)** TG thermograms of PNCs, **(b)** DSC curves (cooling) of PNCs showing $T_g$ and **(c)** DSC curves (heating) of PNCs showing $T_m$. #Data presented from Chapter 3 for comparison.

### 7.3.6. Shape memory behavior

Shape memory behavior of polymeric material can be considered as an entropic effect.[28,37] Under normal condition, polymer resides a permanent macroscopic shape in which polymeric chains tend to orient themselves in a random coil formation. Such state corresponds to the maximum entropy of the polymeric chains leading to a thermodynamically stable stage. However, upon heating the polymeric system above $T_{trans}$ ($T_{trans}$+20 °C in the present case), the chain mobility increases significantly.[28] Application of external force under such condition leads to a conformational change, which results a deformed temporary state. The whole process is accompanied by lowering of entropy.[28] This lower entropy state is kinetically entrapped by freezing the polymeric chain segments in an ice cool condition. This ultimately results fixation of the temporary shape. The permanent shape can be successfully retrieved by heating above $T_{trans}$. All the polymeric nanocomposites found to possess good shape memory behavior. It was found that with increase amount of $NiFe_2O_4$@rGO content, shape recovery time decreased (**Table 7.2**). This can be ascribed to the high thermal conductivity of rGO, which facilitates an effective heating throughout the polymer matrix resulting random orientation of the polymeric chain with maximum entropy.[27] On the other hand, all the polymeric nanocomposites responded effectively towards the non-contact, external stimuli like sunlight and microwave. It is mainly due to the presence of $NiFe_2O_4$@rGO nano-filler within the polymer matrix. $NiFe_2O_4$@rGO contains

**Table 7.2.** Shape memory parameters of WHPU/$NiFe_2O_4$@rGO nanocomposite

| Stimulus | Shape memory parameter | PNC0.5 | PNC1.0 | PNC1.5 | PNC2.0 |
|---|---|---|---|---|---|
| **Microwave** | Recovery time (s) | 72 | 60 | 53 | 40 |
| | Shape recovery (%) | 96.9 | 97.3 | 97.6 | 98.4 |
| | Shape fixity (%) | 94.2 | 95.3 | 96.4 | 96.9 |
| **Sunlight** | Recovery time (s) | 170 | 150 | 135 | 115 |
| | Shape recovery (%) | 93.2 | 93.5 | 94.2 | 95.3 |
| | Shape fixity (%) | 94.2 | 95.3 | 96.4 | 96.9 |
| **Thermal** | Recovery time (s) | 90 | 82 | 75 | 60 |
| | Shape recovery (%) | 96.5 | 97.1 | 97.8 | 98.6 |
| | Shape fixity (%) | 94.2 | 95.3 | 96.4 | 96.9 |

both magnetic and electrically active components. Hence, $NiFe_2O_4$@rGO/WHPU nanocomposite undergo strong interaction with electromagnetic radiations like microwave or even with normal sunlight.[38] It is a known fact that $NiFe_2O_4$/graphene based nanohybrid system can absorb microwave energy.[39] It is also very active under normal sunlight condition.[40] As a result, it strongly absorbs when exposed to microwave or sunlight, which can stimulate an indirect but effective heating within the polymer matrix. The study showed that microwave irradiation of the deformed nanocomposite films at 300 W is good enough to retrieve the original shapes within a minute (**Figure 7.7**). However, under normal sunlight with flux density 80,000-90,000 lux, WHPU/$NiFe_2O_4$@rGO took little longer time for shape recovery. Nevertheless, in both the cases effective shape recovery time was recorded. All the shape memory parameters are shown in **Table 7.2**. Similar to the thermally induced shape recovery, a dose dependent lowering of shape recovery time was witnessed under microwave and sunlight triggers.

## 7.4. Conclusion

From the study inference can be made that nickel ferrite decorated reduced graphene oxide can be effectively used in the *in situ* fabrication of waterborne

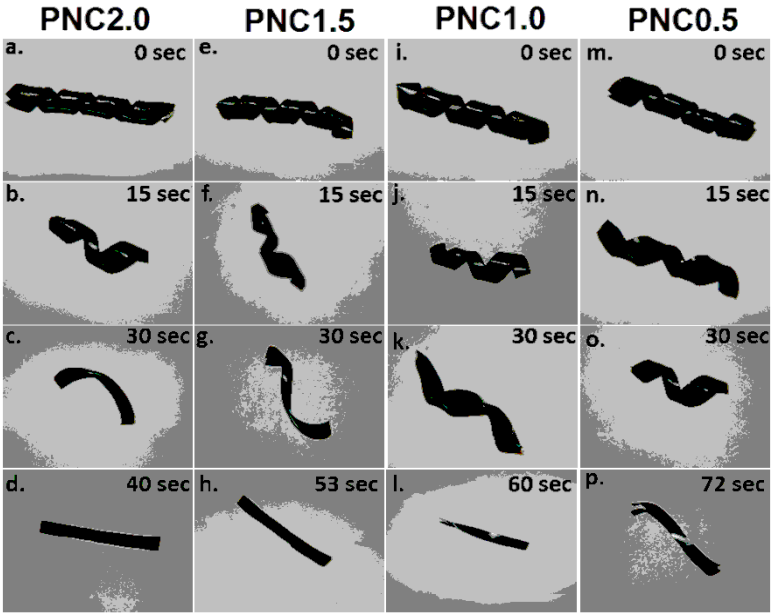


**Figure 7.7.** Shape memory behavior of PNCs under microwave (300 W) irradiation.

polyurethane system. Such an approach may be effective to overcome poor compatibility problem of polyurethane with graphene-based nanomaterials. The study showed that all the compositions of the polymeric nanocomposite possess high mechanical properties and thermal stability. Such high performance is attributed to the uniform distribution of nanomaterial over the polymer matrix. In addition to that, developed nanocomposite demonstrated multi-stimuli responsive shape memory behavior. Microwave and sunlight radiations are successfully utilized as nano-contact and remote trigger in the shape recovery process. Thus, such a system can be used as low VOC containing, eco-friendly material with high performance and shape memory ability for their allied applications.

**References**

(1) Lee, C., et al. Measurement of the elastic properties and intrinsic strength of monolayer graphene, *Science* **321**, 385--388, 2008.

(2) Balandin, A.A., et al. Superior thermal conductivity of single-layer graphene, *Nano Lett.* **8**, 902--907, 2008.

(3) Morozov, S.V., et al. Giant intrinsic carrier mobilities in graphene and its bilayer, *Phys. Rev. Lett.* **100**, 016602 (4 pp), 2008.

(4) Bonaccorso, F., et al. Graphene photonics and optoelectronics, *Nat. Photonics* **4**, 611--622, 2010.

(5) Zhao, Q., et al. Recent progress in shape memory polymer: New behavior, enabling materials, and mechanistic understanding, *Prog. Polym. Sci.* **49**, 79--120, 2015.

(6) Liu, Y., et al. Shape memory polymers and their composites in aerospace applications: A review, *Smart Mater. Struct.* **23**, 023001, 2014.

(7) Singhal, P., et al. Low density biodegradable shape memory polyurethane foams for embolic biomedical applications, *Acta Biomater.* **10**, 67--76, 2014.

(8) Hu, J. *Shape Memory Polymers and Textiles*, Woodhead Publishing Limited, Cambridge, 2007.

(9) Behl, M., & Lendlein, A. Shape-memory polymers, *Mater. Today* **10**, 20--28, 2007.

(10) Hu, J., et al. Recent advances in shape–memory polymers: Structure, mechanism, functionality, modeling and applications, *Prog. Polym. Sci.* **37**, 1720--1763, 2012.

(11) Thakur, S., & Karak, N. Bio-based tough hyperbranched polyurethane-graphene oxide nanocomposites as advanced shape memory materials, *RSC Adv.* **3**, 9476--9482, 2013.

(12) Takahashi, T., et al. Structure and properties of shape-memory polyurethane block copolymers, *J. Appl. Polym. Sci.* **60**, 1061--1069, 1996.

(13) Lee, B.S., et al. Structure and thermomechanical properties of polyurethane block copolymers with shape memory effect, *Macromolecules* **34**, 6431--6437, 2001.

(14) Meng, H., & Li, G. A review of stimuli-responsive shape memory polymer composites, *Polymer* **54**, 2199--2221, 2013.

(15) Liu, F., & Urban, M.W. Recent advances and challenges in designing stimuli-responsive polymers, *Prog. Polym. Sci.* **35**, 3--23, 2010.

(16) Yan, X., et al. Stimuli-responsive supramolecular polymeric materials, *Chem. Soc. Rev.* **41**, 6042--6065, 2012.

(17) Lendlein, A., & Kelch, S. Shape-memory polymers as stimuli-sensitive implant materials, *Clin. Hemorheol. Micro.* **32**, 105--116, 2005.

(18) Dong, S., et al. A crown ether appended super gelator with multiple stimulus responsiveness, *Adv. Mater.* **24**, 3191--3195, 2012.

(19) Kalita, H., & Karak, N. Hyperbranched polyurethane/$Fe_3O_4$ thermosetting nanocomposites as shape memory materials, *Polym. Bull.* **70**, 2953--2965, 2013.

(20) Cho, J.W., et al. Electroactive shape-memory polyurethane composites incorporating carbon nanotubes, *Macromol. Rapid Commun.* **26**, 412--416, 2005.

(21) Leng, J., et al. Electroactivate shape-memory polymer filled with nanocarbon particles and short carbon fibers, *Appl. Phys. Lett.* **91**, 144105, 2007.

(22) Thakur, S., & Karak, N. Bio-based tough hyperbranched polyurethane–graphene oxide nanocomposites as advanced shape memory materials, *RSC Adv.* **3**, 9476--9482, 2013.

(23) Liu, Y., et al. Review of electro-active shape-memory polymer composite, *Compos. Sci. Technol.* **69**, 2064--2068, 2009.

(24) Gunes, I.S., et al. Evaluation of nanoparticulate fillers for development of shape memory polyurethane nanocomposites, *Polymer* **49**, 2223--2234, 2008.

(25) Leng, J., et al. Infrared light-active shape memory polymer filled with nanocarbon particles, *J. Appl. Polym. Sci.* **114**, 2455--2460, 2009.

(26) Liu, X., et al. Electro-active shape memory composites enhanced by flexible carbon nanotube/graphene aerogels, *J. Mater. Chem. A* **3**, 11641--11649, 2015.

(27) Thakur, S., & Karak, N. Multi-stimuli responsive smart elastomeric hyperbranched polyurethane/reduced graphene oxide nanocomposites, *J. Mater. Chem. A* **2**, 14867--14875, 2014.

(28) Duarah, R., et al. Sustainable starch modified polyol based tough, biocompatible, hyperbranched polyurethane with a shape memory attribute, *New J. Chem.* **40**, 5152--5163, 2016.

(29) Kumar, S., et al. Modeling of formation of gold nanoparticles by citrate method, *Ind. Eng. Chem. Res.* **46**, 3128--3136, 2007.

(30) Larciprete, R., et al. Dual path mechanism in the thermal reduction of graphene oxide, *J. Am. Chem. Soc.* **133**, 17315--17321, 2011.

(31) Umapathy, G., et al. Investigation on combustion synthesis of nanocyrstalline nickel ferrite using sodium azide as a potential fuel, *Int. J. Chem. Tech. Res.* **7**, 131--137, 2015.

(32) Maensiri, S., et al. A simple route to synthesize nickel ferrite ($NiFe_2O_4$) nanoparticles using egg white, *Scr. Mater.* **56**, 797--800, 2007.

(33) Liu, H., et al. Simultaneous reduction and surface functionalization of graphene oxide for hydroxyapatite mineralization, *J. Phy. Chem. C* **116**, 3334--3341, 2012.

(34) Sivakumar, P., et al. Preparation and properties of nickel ferrite ($NiFe_2O_4$) nanoparticles via sol–gel auto-combustion method, *Mater. Res. Bull.* **46**, 2204--2207, 2011.

(35) Matei, A., et al. Synthesis and characterization of ZnO–polymer nanocomposites, *Int. J. Mater. Form.* **1**, 767--770, 2008.

(36) Hsiao, S.T., et al. Effect of covalent modification of graphene nanosheets on the electrical property and electromagnetic interference shielding performance of a water-borne polyurethane composite, *ACS Appl. Mater. interfaces* **7**, 2817--2826, 2015.

(37) Xie, T. Recent advances in polymer shape memory, *Polymer* **52**, 4985--5000, 2011.

(38) Chen, Z., et al. Lightweight and Flexible Graphene Foam Composites for High-Performance Electromagnetic Interference Shielding, *Adv. Mater.* **25**, 1296--1300, 2013.

(39) Fu, M., et al. Preparation of $NiFe_2O_4$ nanorod–graphene composites via an ionic liquid assisted one-step hydrothermal approach and their microwave absorbing properties, *J. Mater. Chem. A* **1**, 5577--5586, 2013.

(40) Fu, Y., et al. Graphene-supported nickel ferrite: A magnetically separable photocatalyst with high activity under visible light, *AIChE J.* **58**, 3298--3305, 2012.